Supporting Information

Halide coordinated homoleptic $[Fe_4S_4X_4]^{2-}$ and heteroleptic $[Fe_4S_4X_2Y_2]^{2-}$ clusters (X, Y = Cl, Br, I) – Alternative preparations, structural analogies and spectroscopic properties in solution and solid state

Andreas O. Schüren,[a,b] Verena K. Gramm,[a] Maximilian Dürr,[c] Ana Foí,[b] Ivana Ivanović-Burmazović,[c] Fabio Doctorovich,[b] Uwe Ruschewitz,[a] and Axel Klein*[a]

Supplementary Figures (Figures S1 – S29)

ESI mass spectrometry

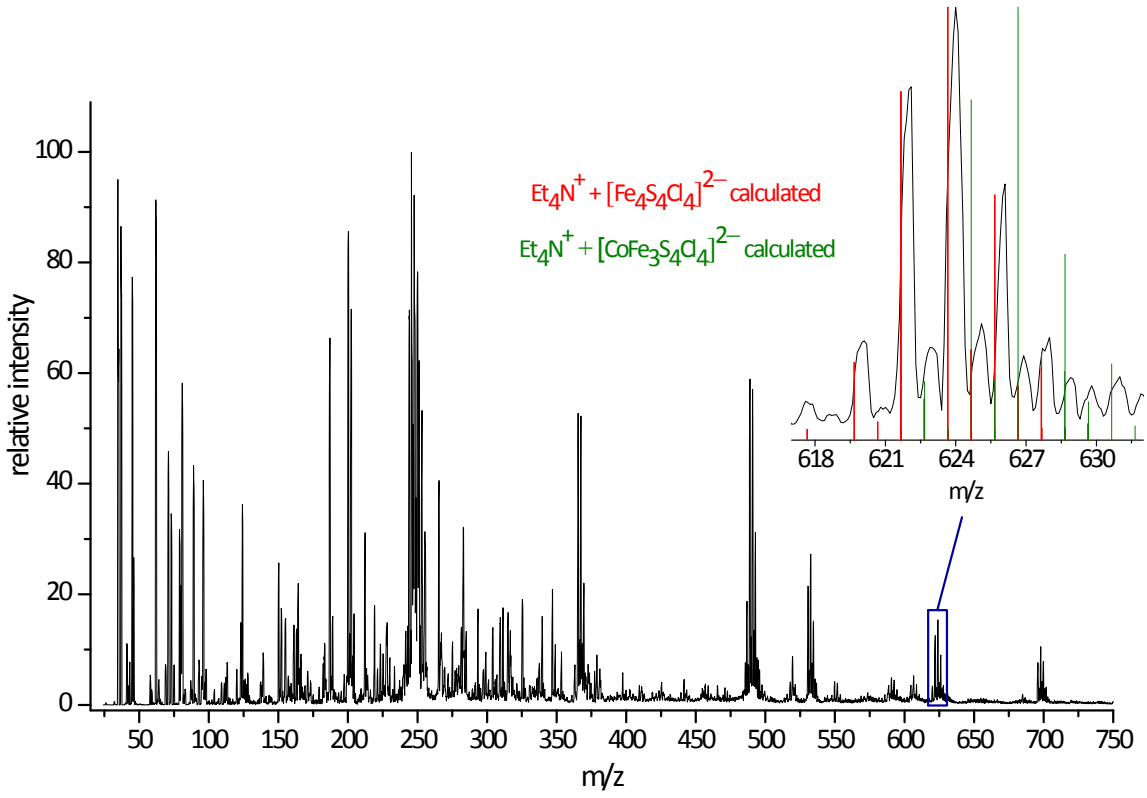

Figure S1: Negative ESI MS of $(Et_4N)_2[Fe_4S_4Cl_4]$ obtained from reaction with $[CoCl_4]^{2-}$ in MeCN.

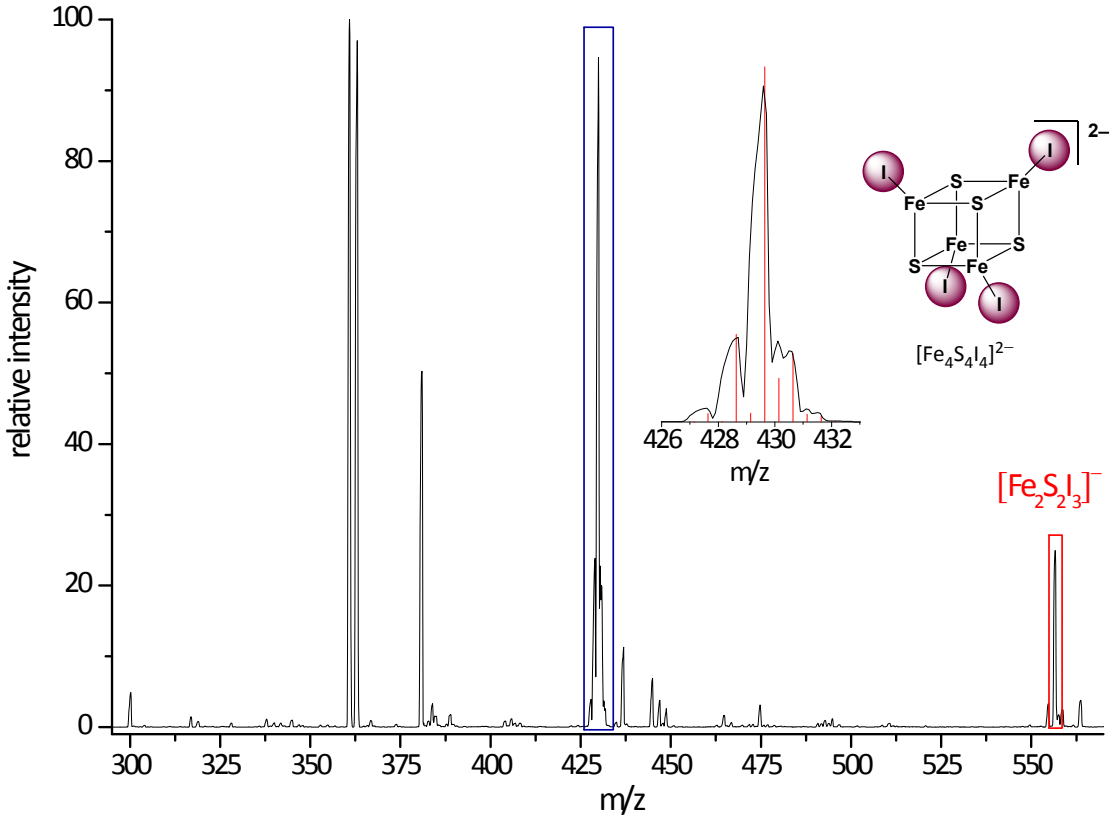

Figure S2: Negative ESI MS of $(BTMA)_2[Fe_4S_4I_4]$ in THF.

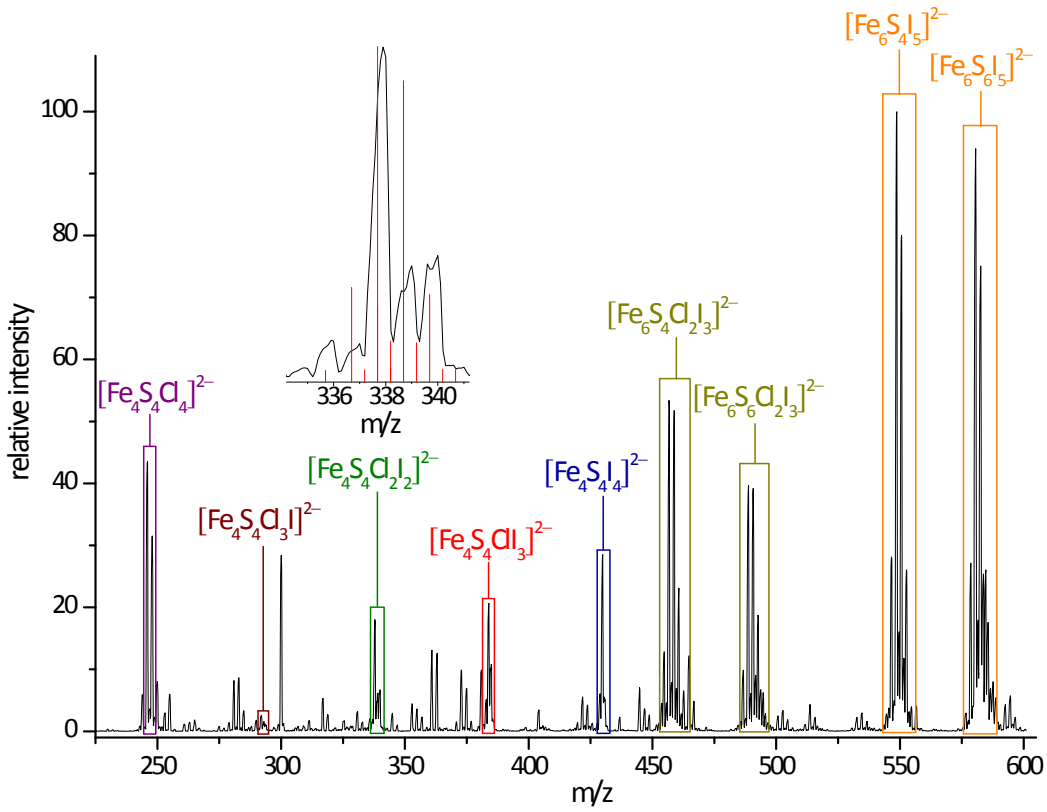

Figure S3: Negative ESI MS of $(BTMA_2[Fe_4S_4Cl_2I_2]$ in THF; conversion with iodine and chloride.

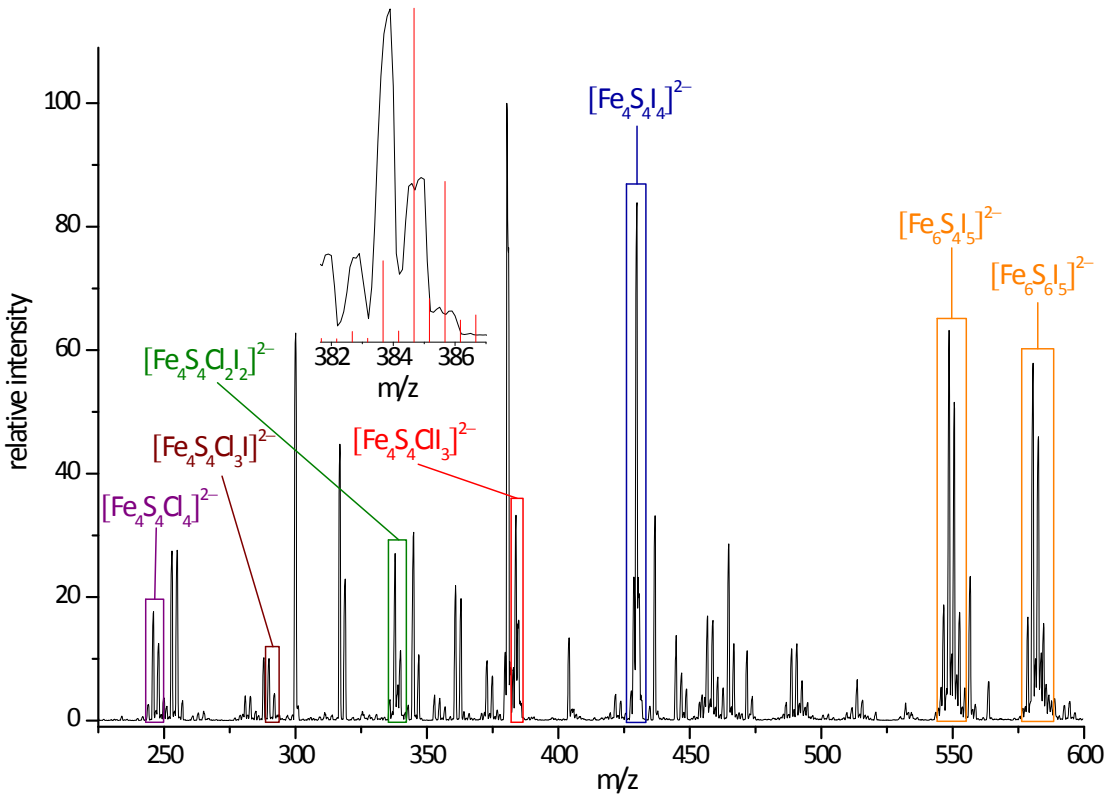

Figure S4: Negative ESI MS of ($BTMA_2[Fe_4S_4ClI_3]$ in THF; conversion with iodine monochloride and iodide.

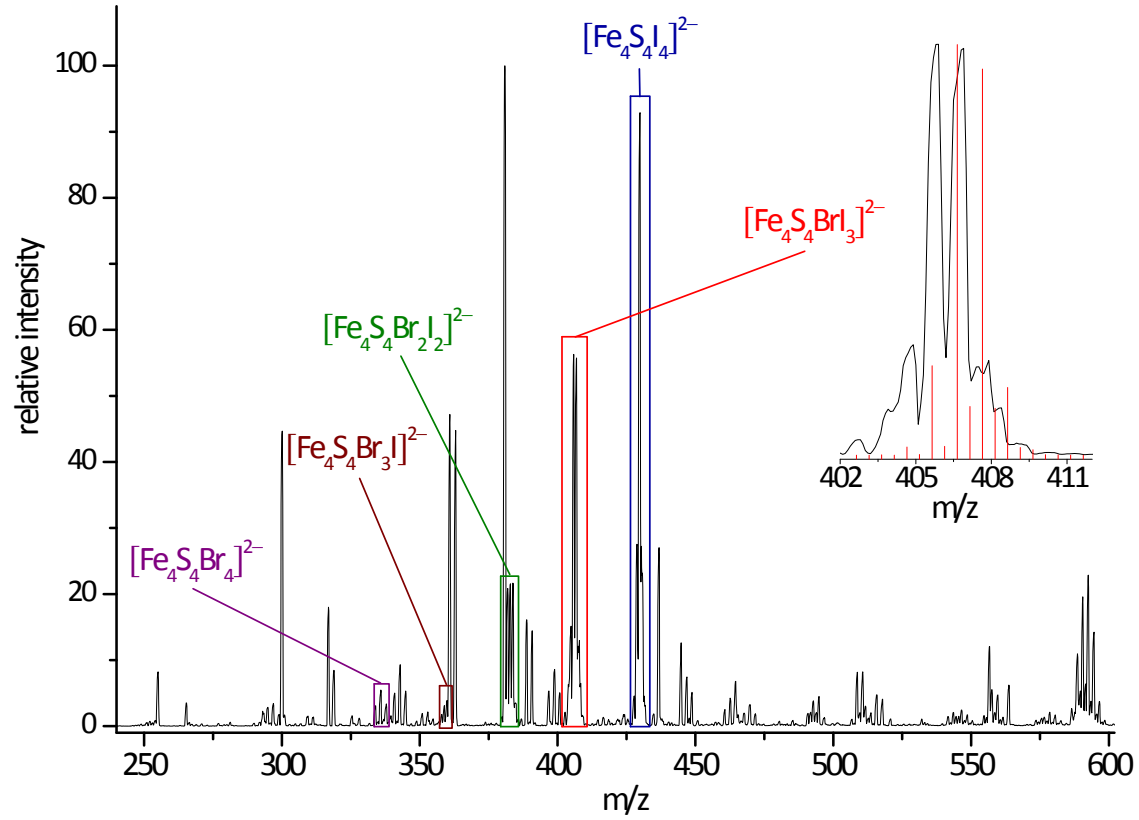

Figure S5: Negative ESI MS of ($BTMA_2[Fe_4S_4BrI_3]$ in THF; conversion with iodine monobromide and iodide.

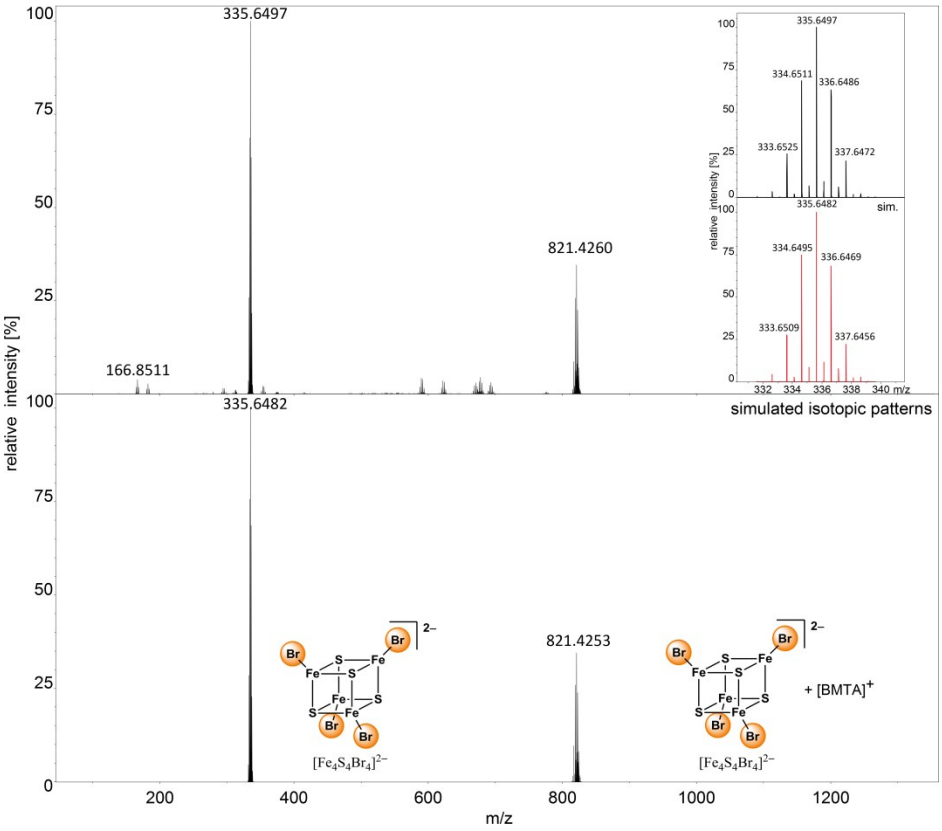

Figure S6: Negative UHR ESI MS of $(BTMA)_2[Fe_4S_4Br_4]$ in acetone (above, measured spectra; below, simulated molecular peaks; detailed view of $[Fe_4S_4Br_4]^{2-}$ with its simulation is given on the right side).

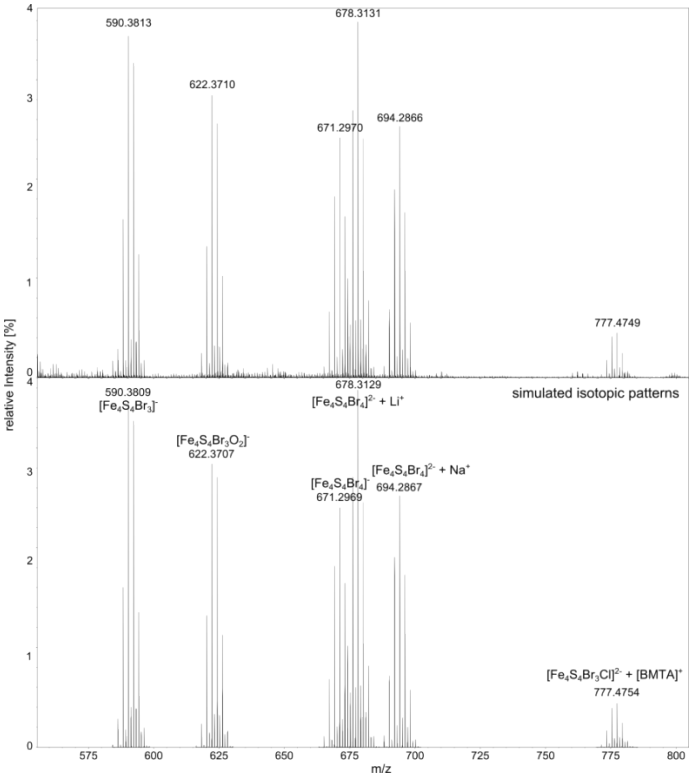

Figure S7: Negative UHR ESI MS of $(BTMA)_2[Fe_4S_4Br_4]$ in acetone and simulated patterns of molecular ions of fragmentation and oxidation products as well as adducts ($[Fe_4S_4Br_3]^-$, $[Fe_4S_4Br_3O_2]^-$, $[Fe_4S_4Br_4]^-$, $[Fe_4S_4Br_3Li]^-$, $[Fe_4S_4Br_3Na]^-$).

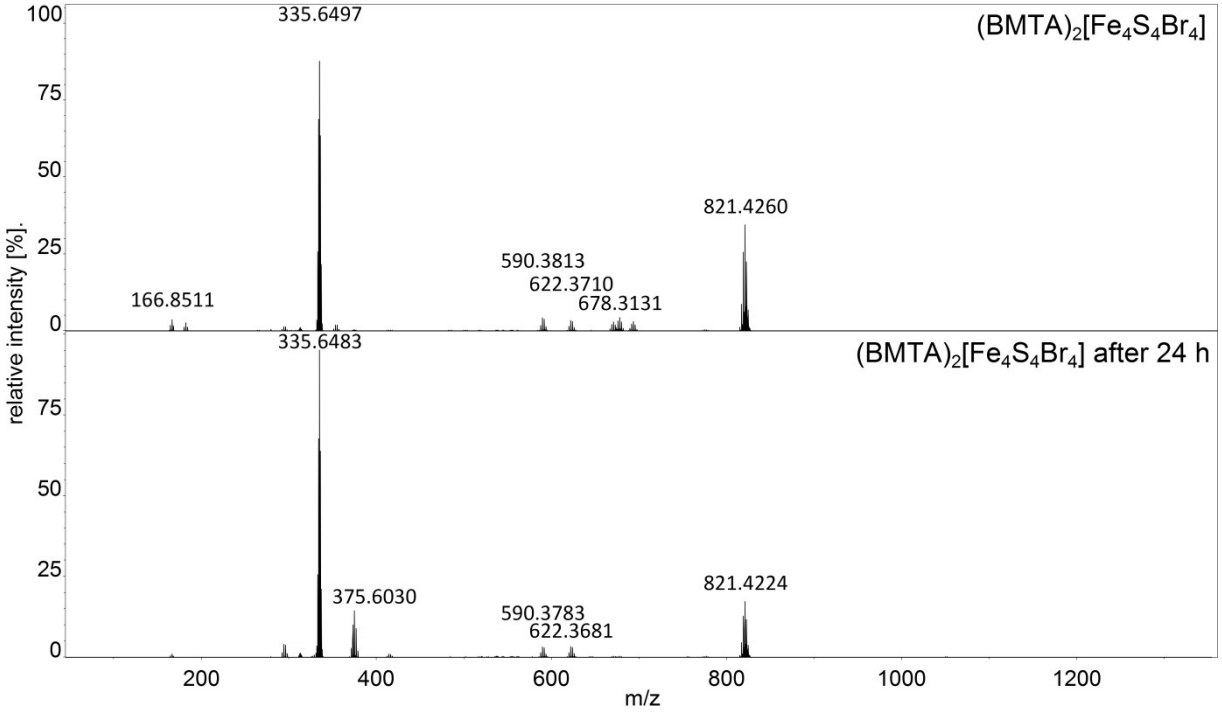

Figure S8: Negative UHR ESI MS of $(BTMA)_2[Fe_4S_4Br_4]$ in acetone (above: measurement after dissolving; below: measurement after 24 h).

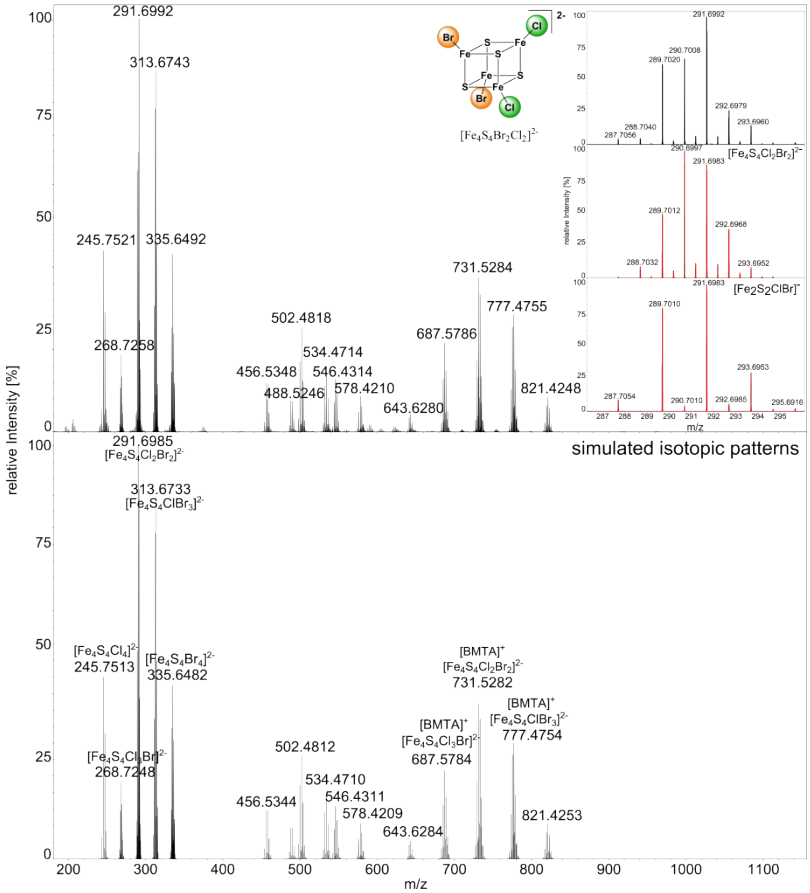

Figure S9: Negative UHR ESI MS of $(BTMA)_2[Fe_4S_4Br_2Cl_2]$ in acetone and simulated patterns of molecular ions.

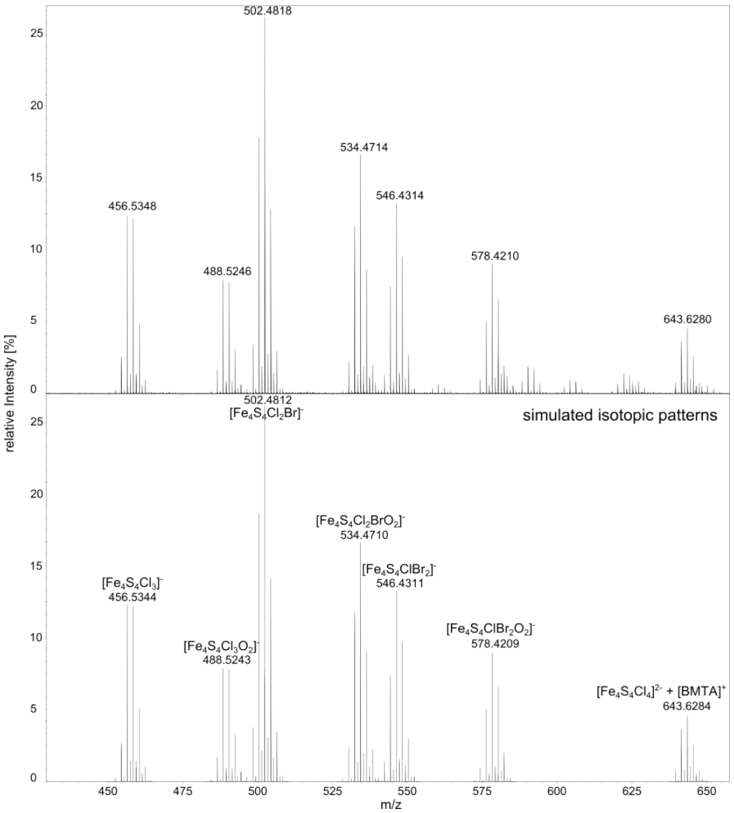

Figure S10: Negative UHR ESI MS of $(BTMA)_2[Fe_4S_4Br_2Cl_2]$ in acetone and simulated patterns of molecular ions; $[Fe_4S_4Br_{3-n}Cl_n]^-$ and $[Fe_4S_4Br_{3-n}Cl_nO_2]^-$ fragmentation series.

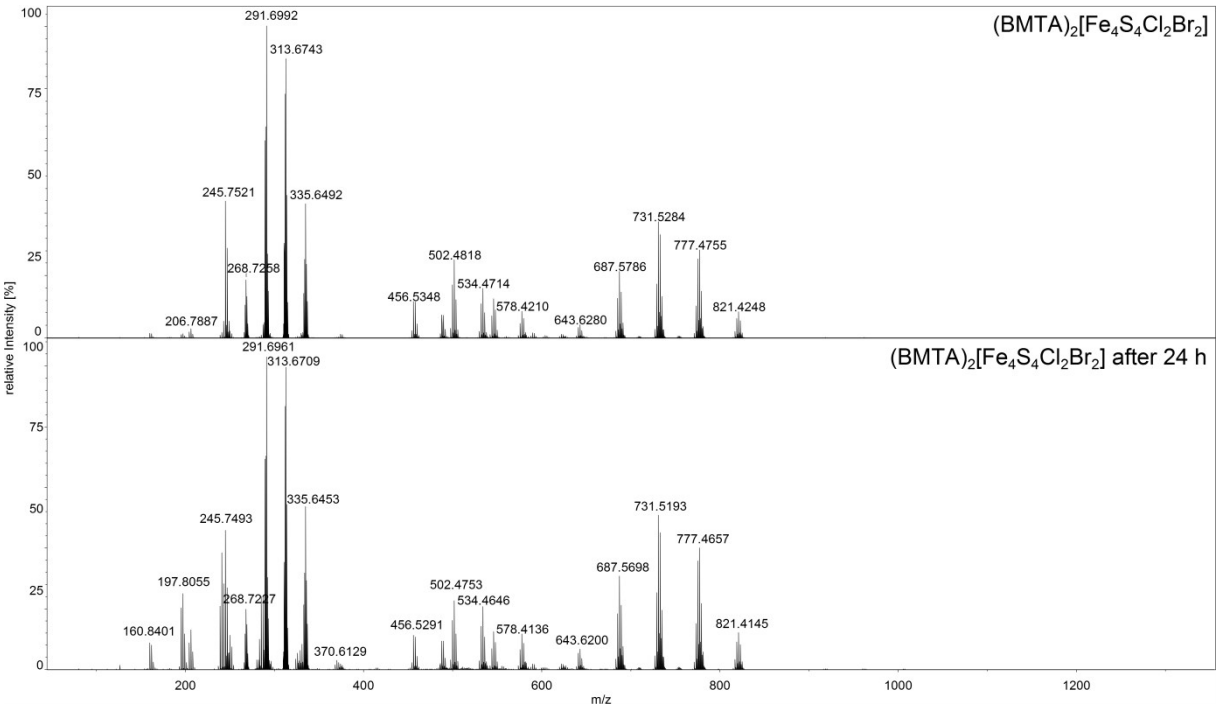

Figure S11: Negative UHR ESI MS of $(BTMA)_2[Fe_4S_4Br_2Cl_2]$ in acetone (top: measurement after dissolving; bottom: measurement after 24 h).

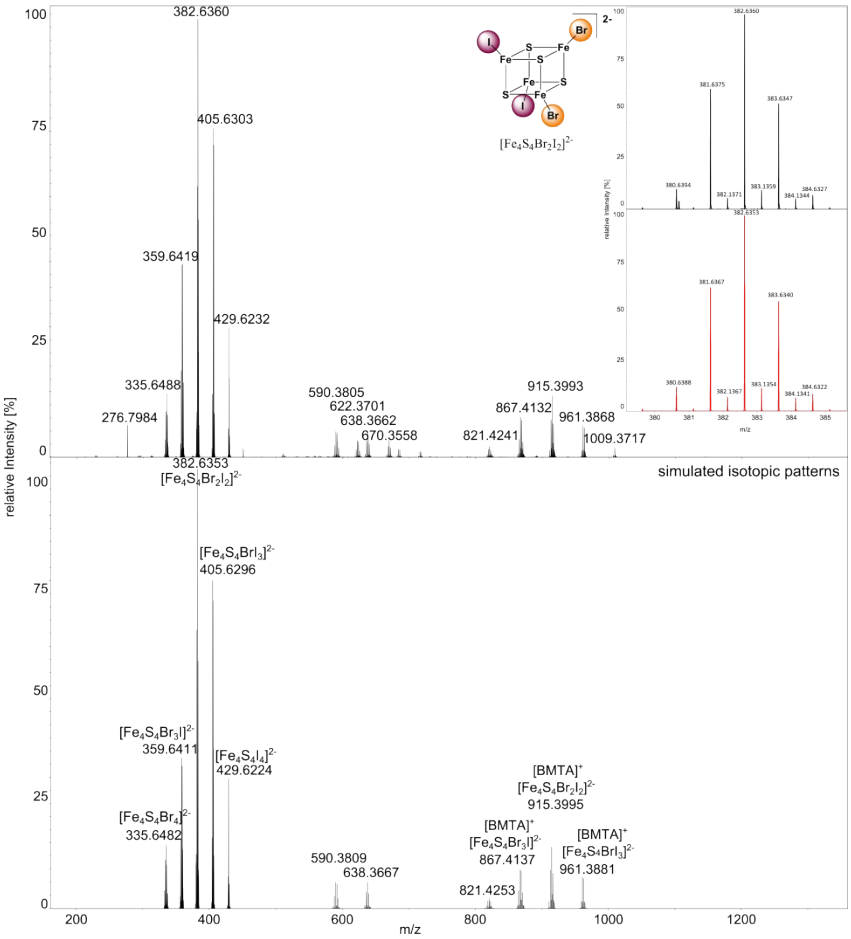

Figure S12: Negative UHR ESI MS of $(BTMA)_2[Fe_4S_4Br_2I_2]$ in acetone and simulated patterns of molecular ions.

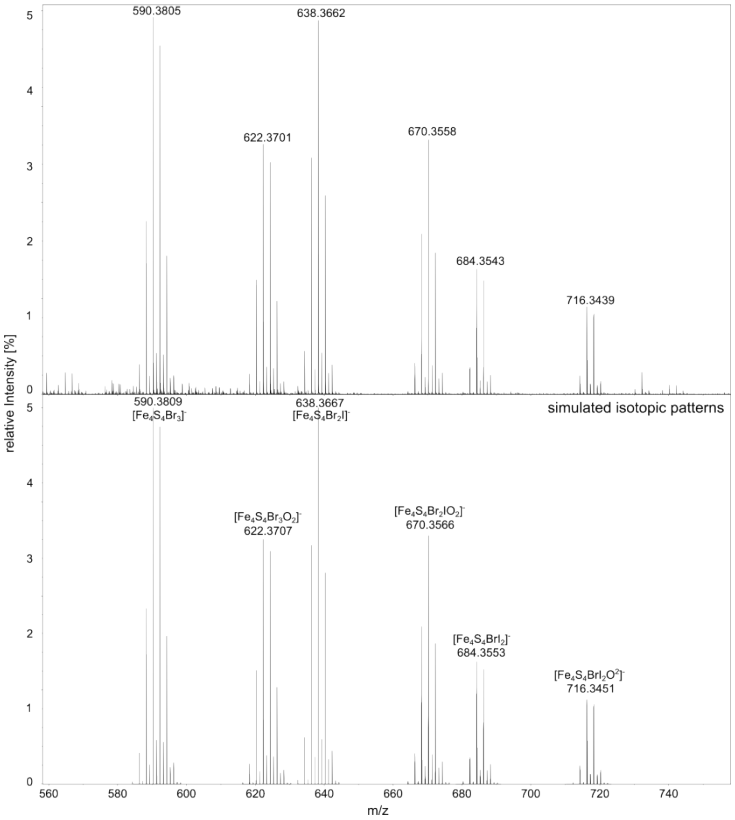

Figure S13: Negative UHR ESI MS of $(BTMA)_2[Fe_4S_4Br_2I_2]$ in acetone and simulated patterns of molecular ions; $[Fe_4S_4Br_{3-n}I_n]^-$ and $[Fe_4S_4Br_{3-n}I_nO_2]^-$ fragmentation series.

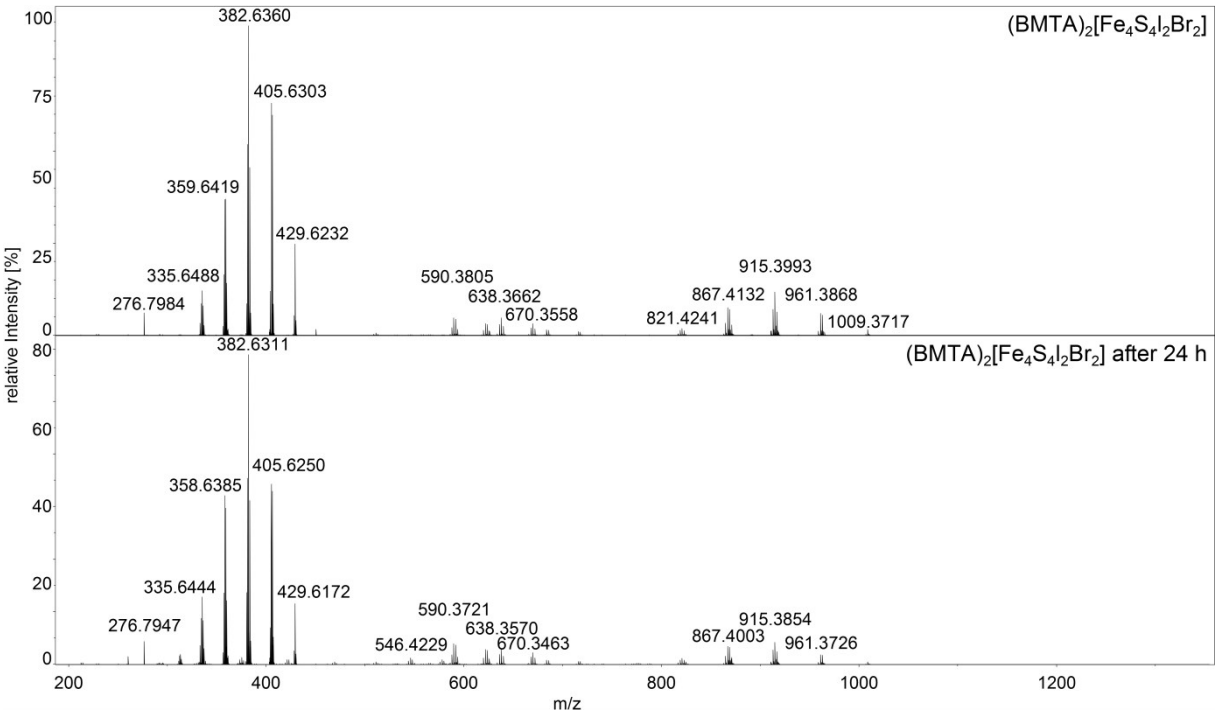

Figure S14: Negative UHR ESI MS of $(BTMA)_2[Fe_4S_4Br_2I_2]$ in acetone (red: measurement after dissolving; green: measurement after 24 h).

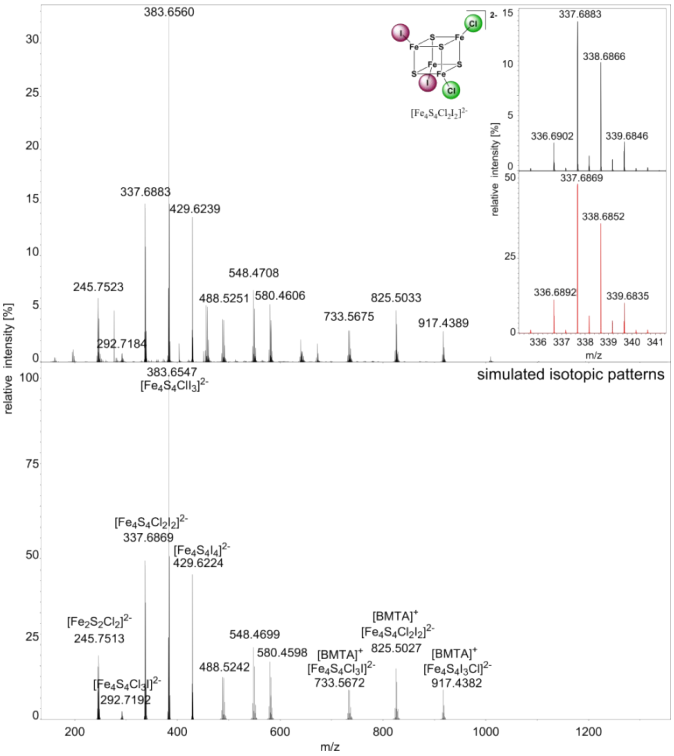

Figure S15: Neg. UHR ESI MS of $(BTMA)_2[Fe_4S_4Cl_2I_2]$ in acetone (above, measured spectra; below, simulated molecular peaks; detailed view of $[Fe_4S_4Cl_2I_2]^{2-}$ with its simulation is given on the right side).

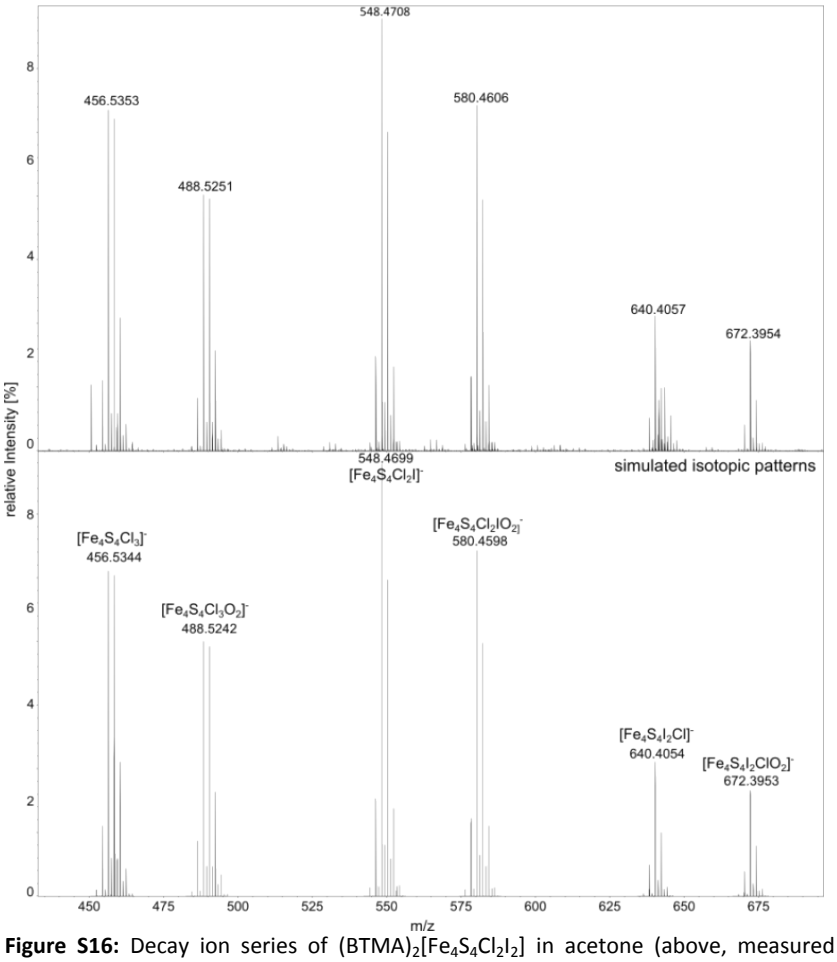

Figure S16: Decay ion series of $(BTMA)_2[Fe_4S_4Cl_2I_2]$ in acetone (above, measured spectra; below, simulated molecular peaks).

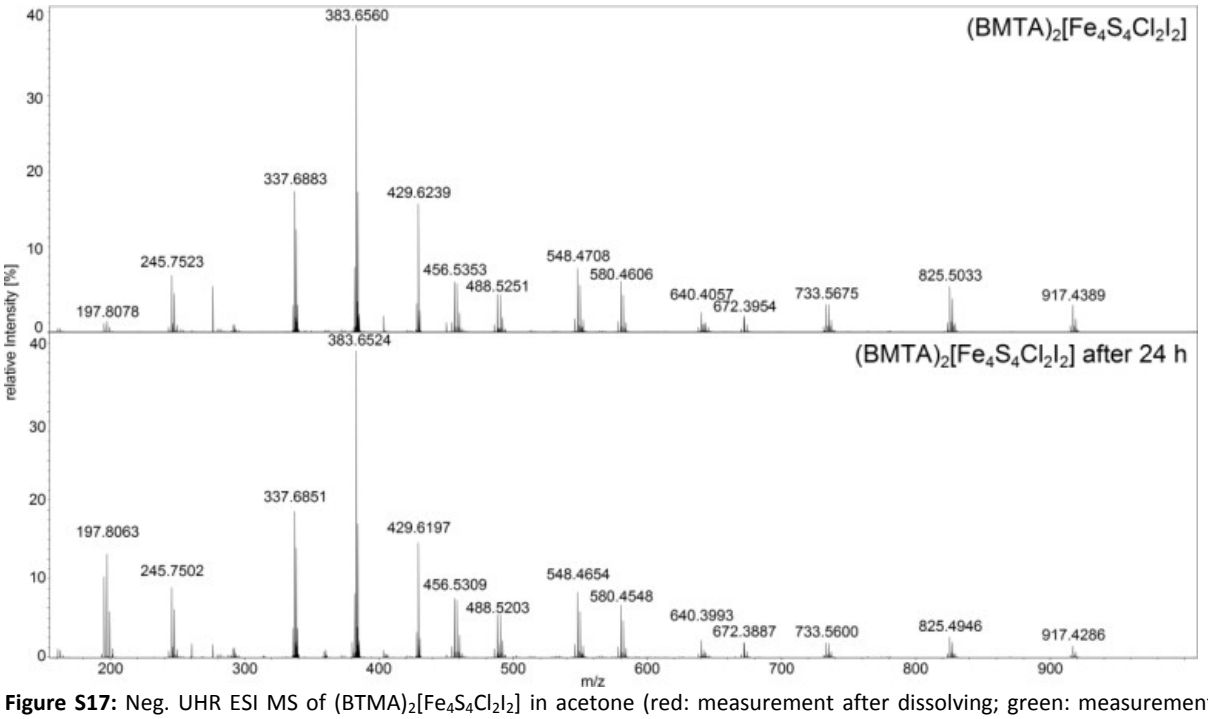

Figure S17: Neg. UHR ESI MS of $(BTMA)_2[Fe_4S_4Cl_2I_2]$ in acetone (red: measurement after dissolving; green: measurement after 24 h).

UV-vis-NIR absorption spectroscopy

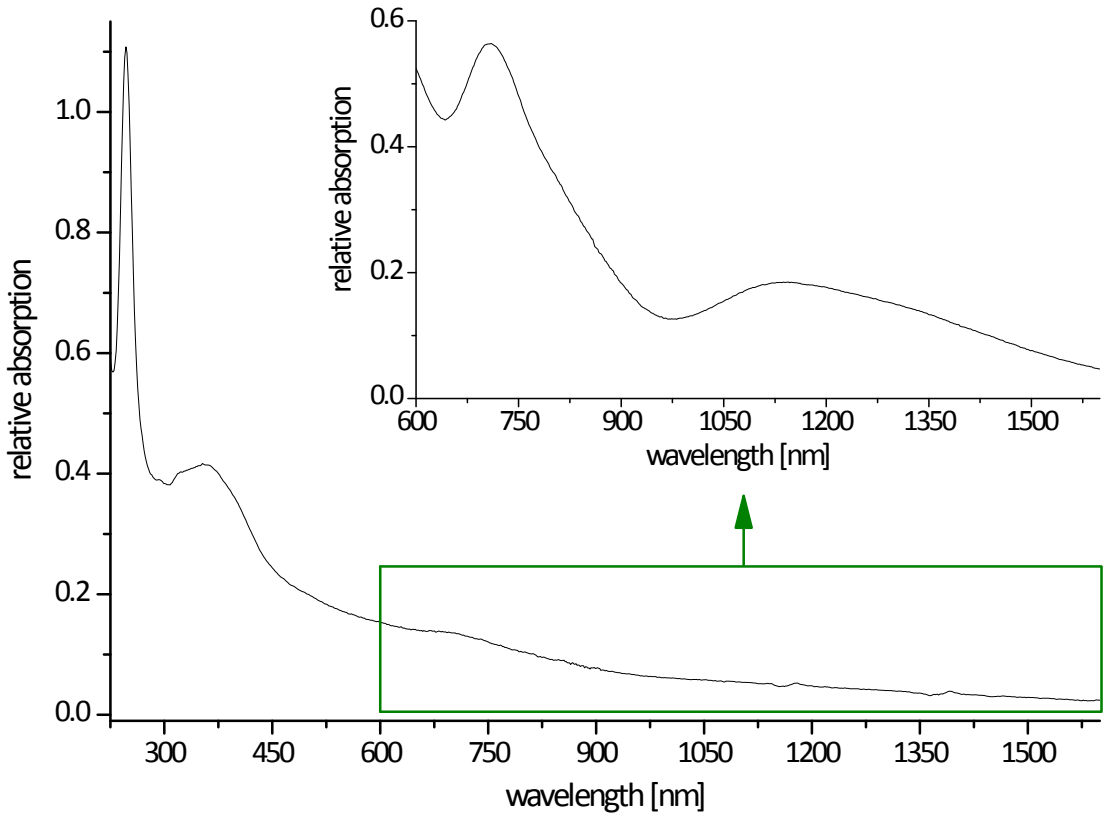

Figure S18: UV-vis-NIR spectra of $(BTMA)_2[Fe_4S_4I_4]$ in acetonitrile.

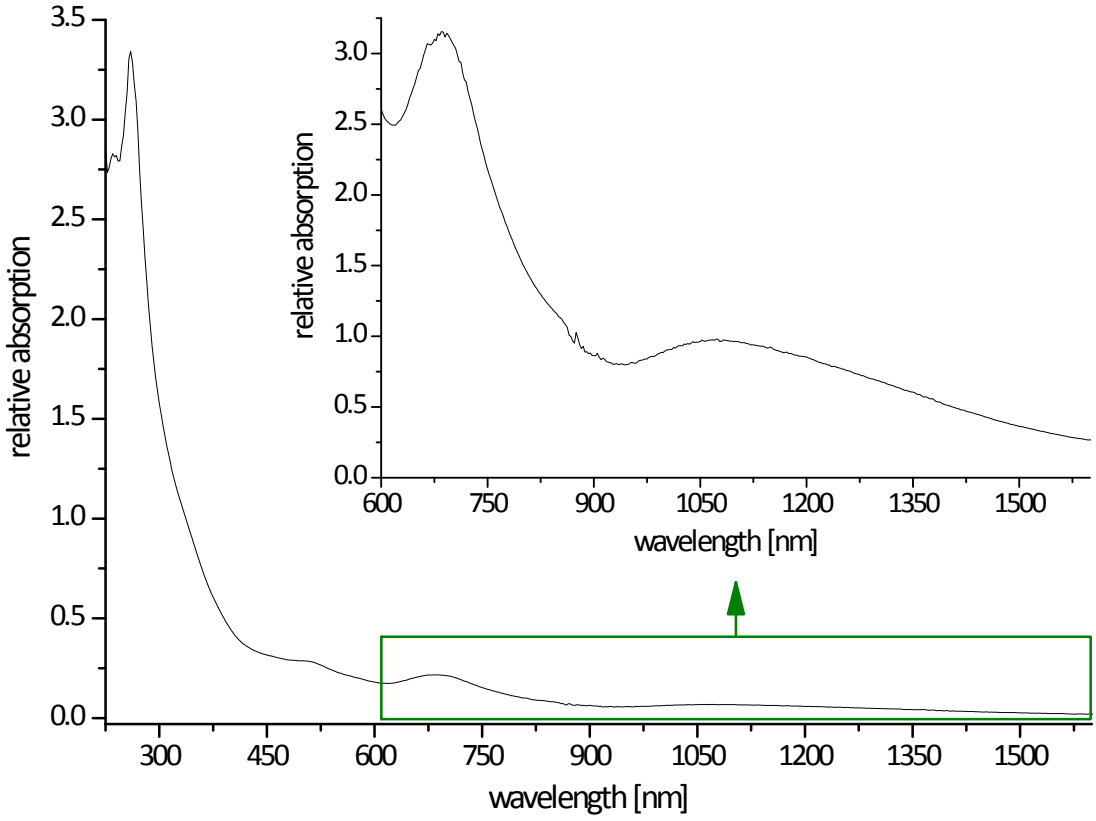

Figure S19: UV-vis-NIR absorption for reaction control during synthesis of $(BTMA)_2[Fe_4S_4Cl_4]$ in acetonitrile.

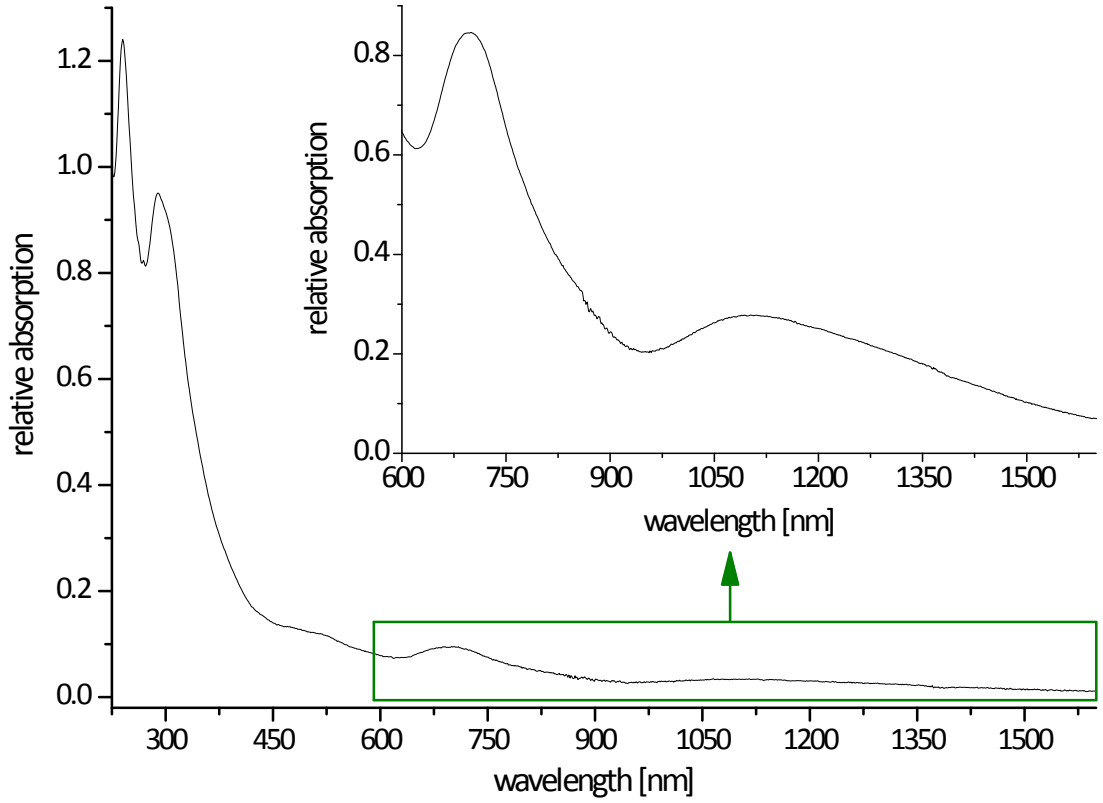

Figure S20: UV-vis-NIR spectra of $(BTMA)_2[Fe_4S_4Br_4]$ in acetonitrile.

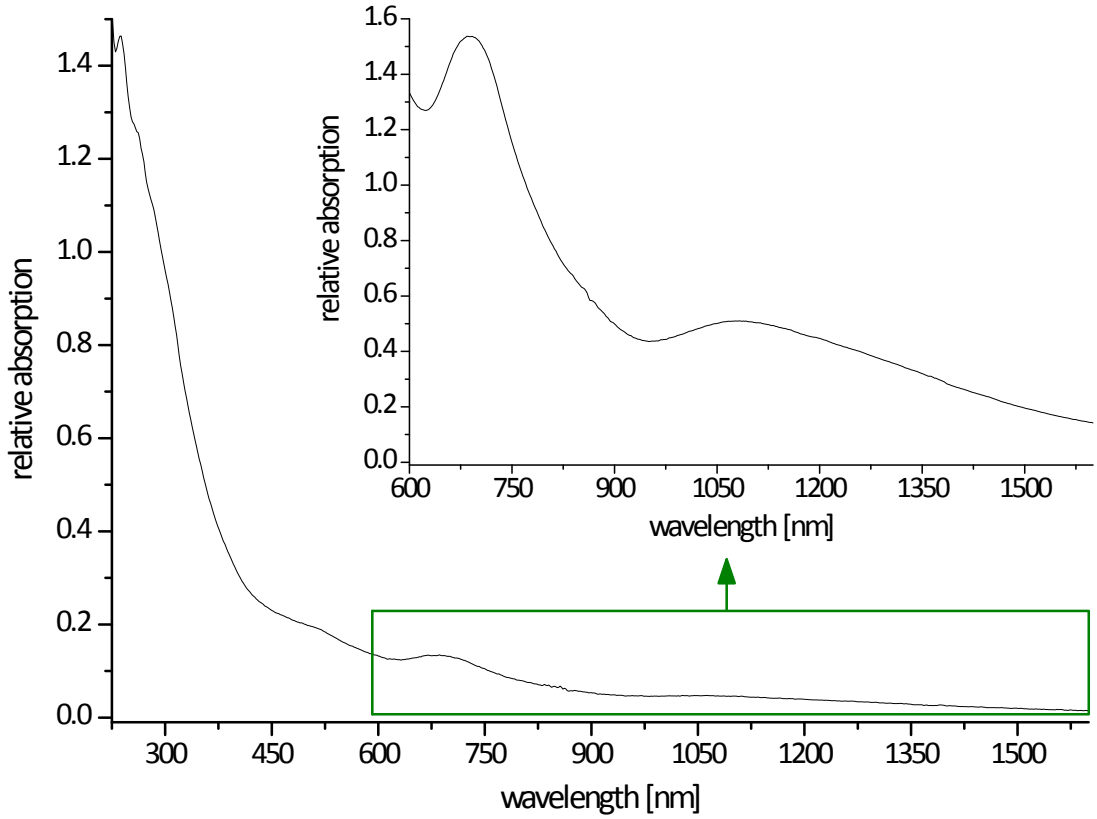

Figure S21: UV-vis-NIR spectra of $(BTMA)_2[Fe_4S_4Br_2Cl_2]$ in acetonitrile.

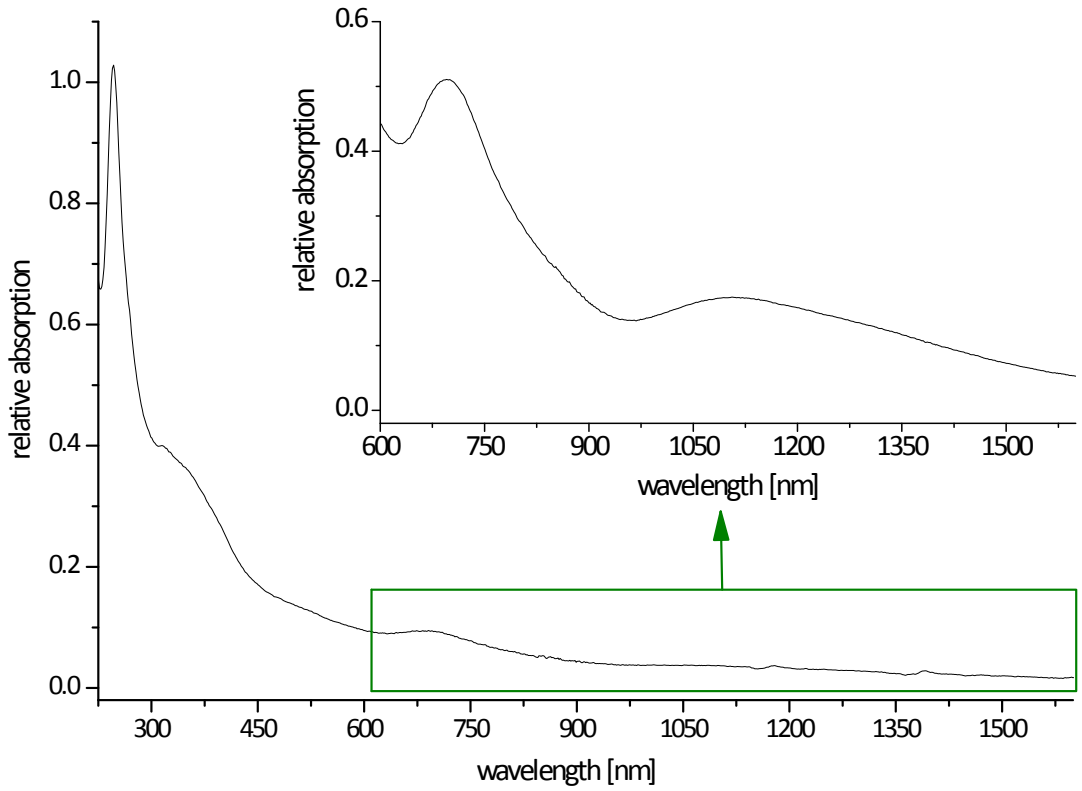

Figure S22: UV-vis-NIR spectra of $(BTMA)_2[Fe_4S_4Cl_2I_2]$ in acetonitrile.

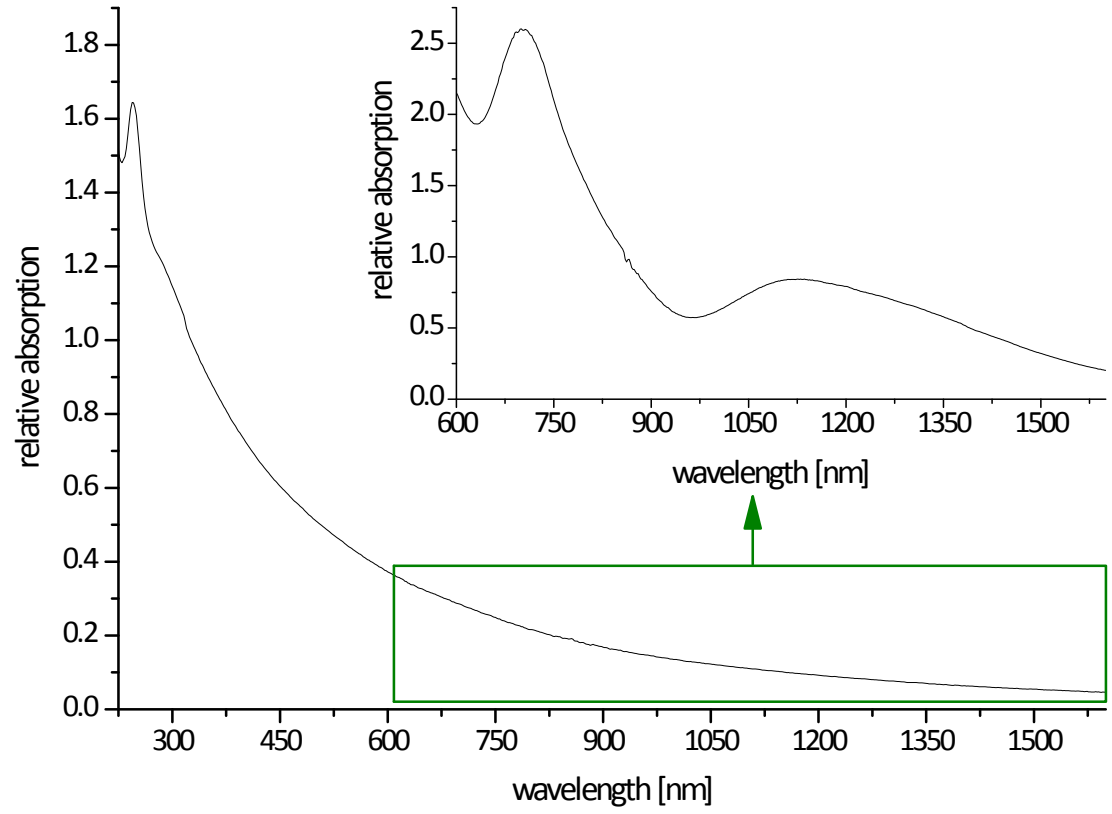

Figure S23: UV-vis-NIR spectra of $(BTMA)_2[Fe_4S_4Br_2I_2]$ in acetonitrile.

Synchrotron X-ray powder diffraction

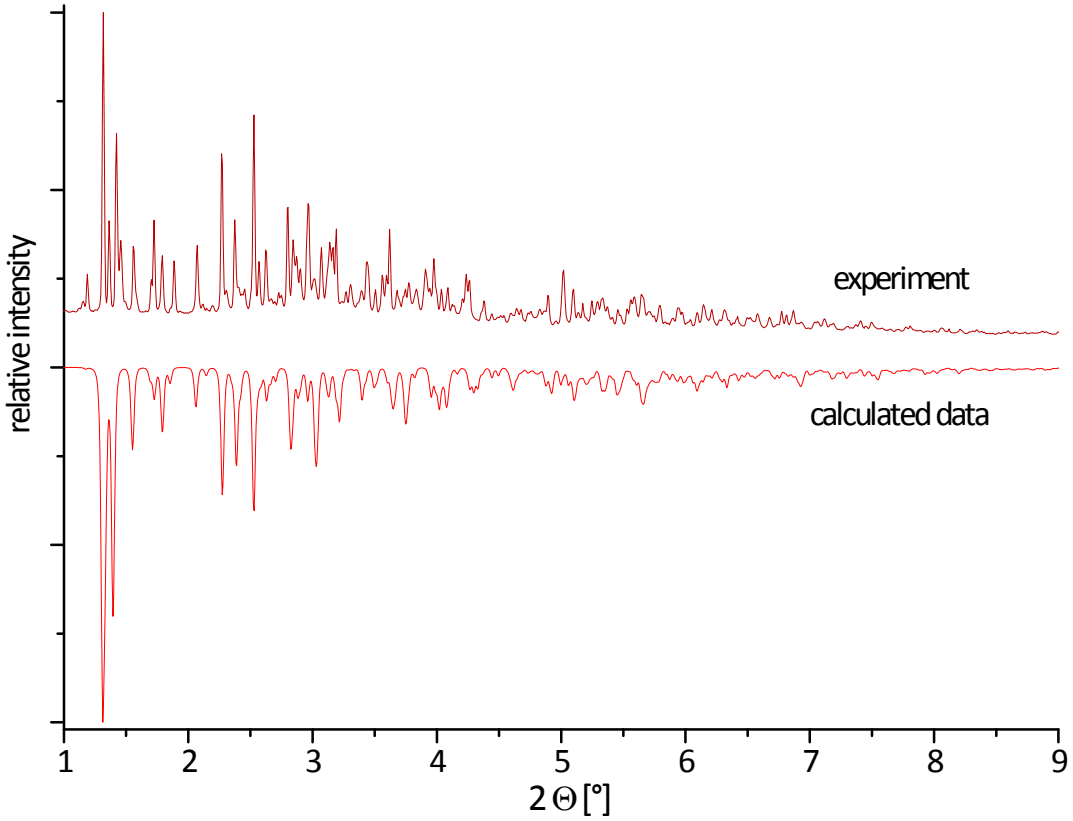

Figure S24: Synchrotron XRPD of $(BTMA)_2[Fe_4S_4I_4]$ at ambient temperature (above: experimental data, with λ = 0.207203 Å; below calculated pattern[1]).

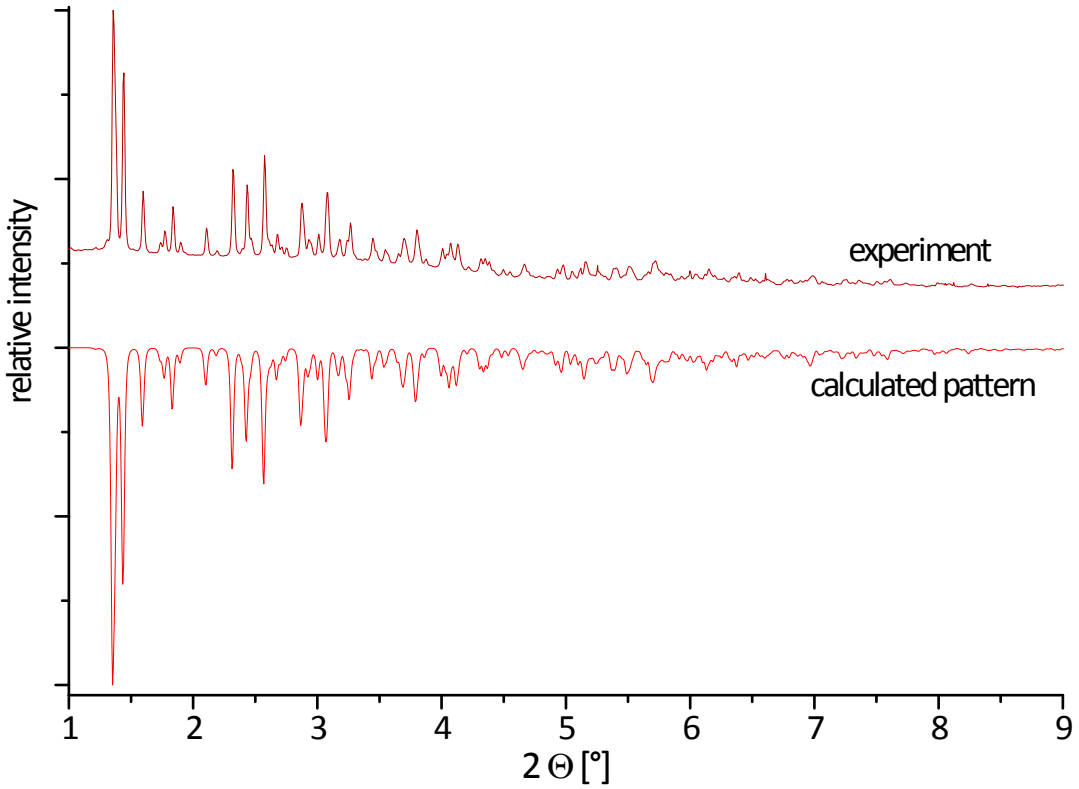

Figure S25: Synchrotron XRPD of $(BTMA)_2[Fe_4S_4Br_4]$ at ambient temperature (above: experimental data, with λ = 0.207203 Å; below calculated pattern[2]).

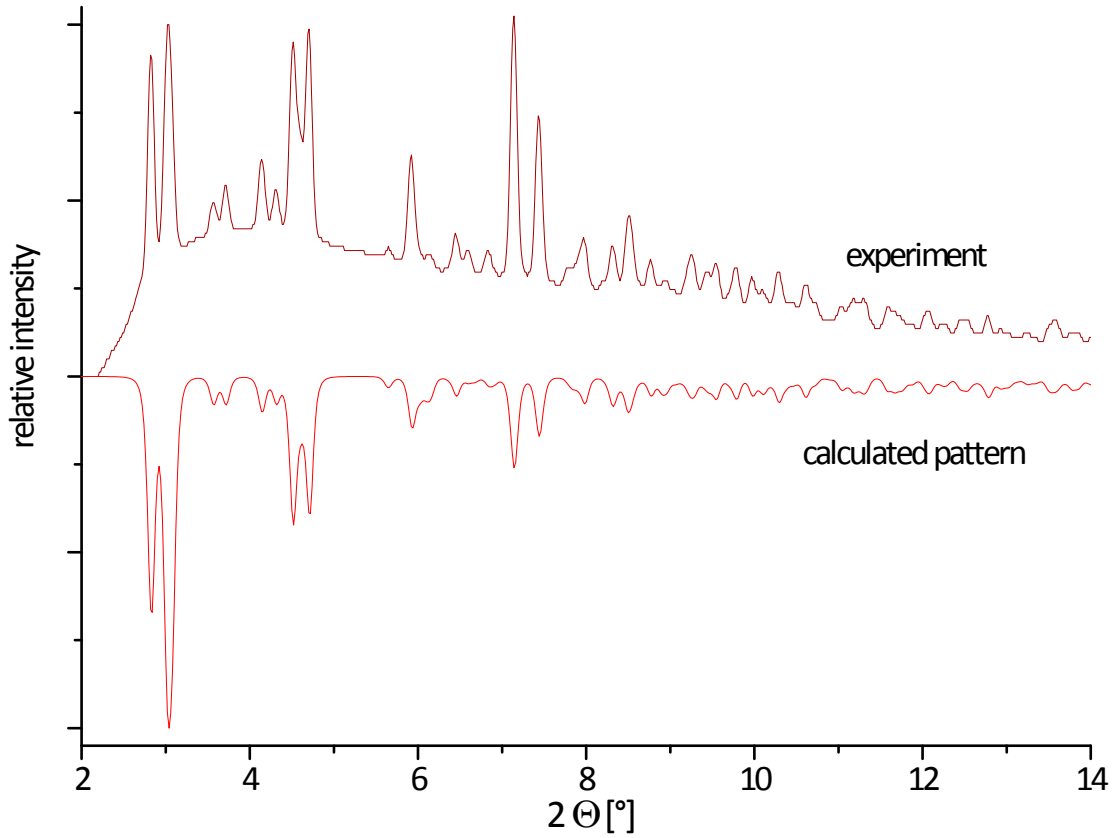

Figure S26: Synchrotron XRPD of $(Ph_4P)_2[Fe_4S_4Br_4]$ at ambient temperature (above: experimental data, with λ = 0.551155 Å; below calculated pattern[3]).

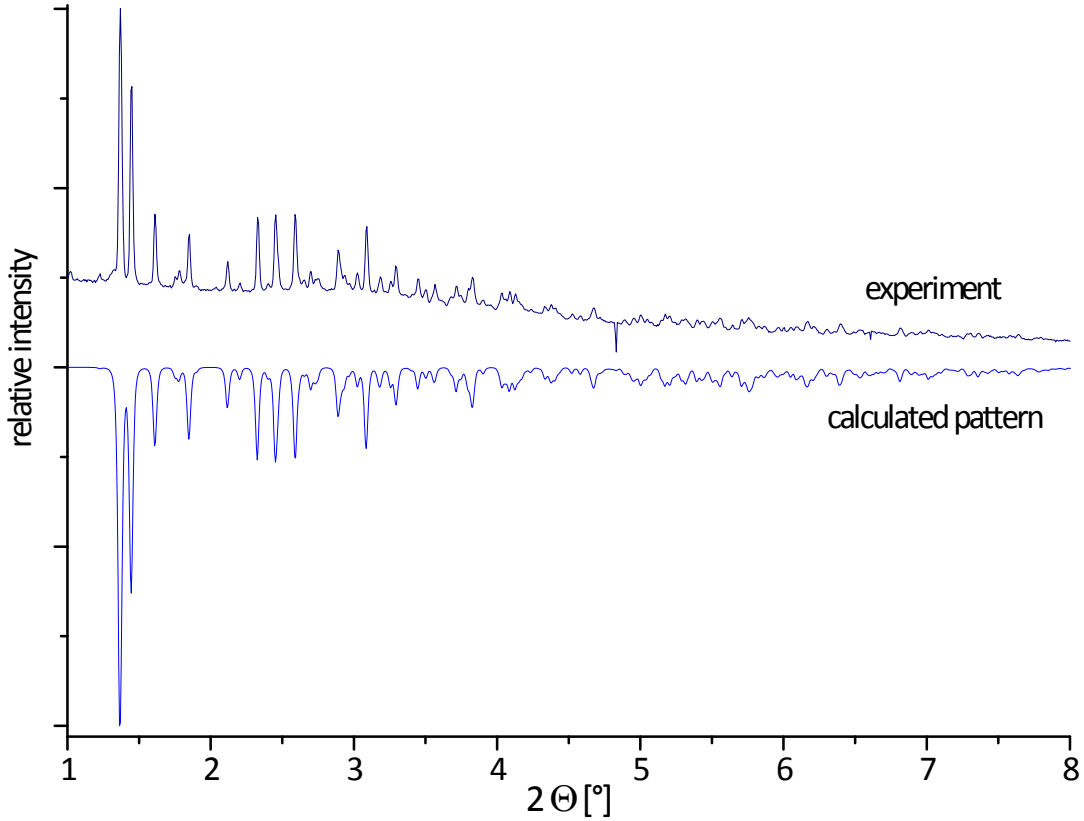

Figure S27: XRPD of $(BTMA)_2[Fe_4S_4Br_2Cl_2]$; experiment with λ = 0.207203 Å synchrotron radiation (DESY, beam line P02.1, storage ring Petra III); calculated pattern based single crystal structure data.[1]

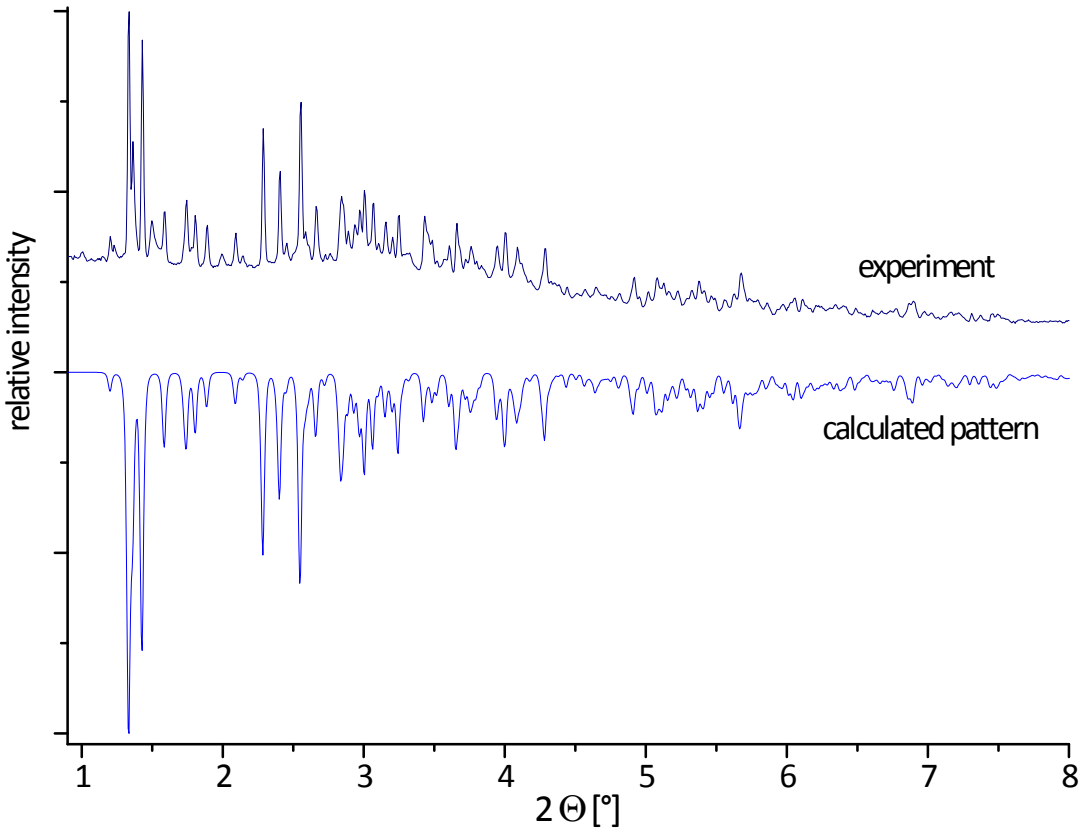

Figure S28: XRPD von $(BTMA)_2[Fe_4S_4Br_2I_2]$; experiment with λ = 0.207203 Å synchrotron radiation (DESY, beam line P02.1, storage ring Petra III); calculated pattern based single crystal structure data.[1]

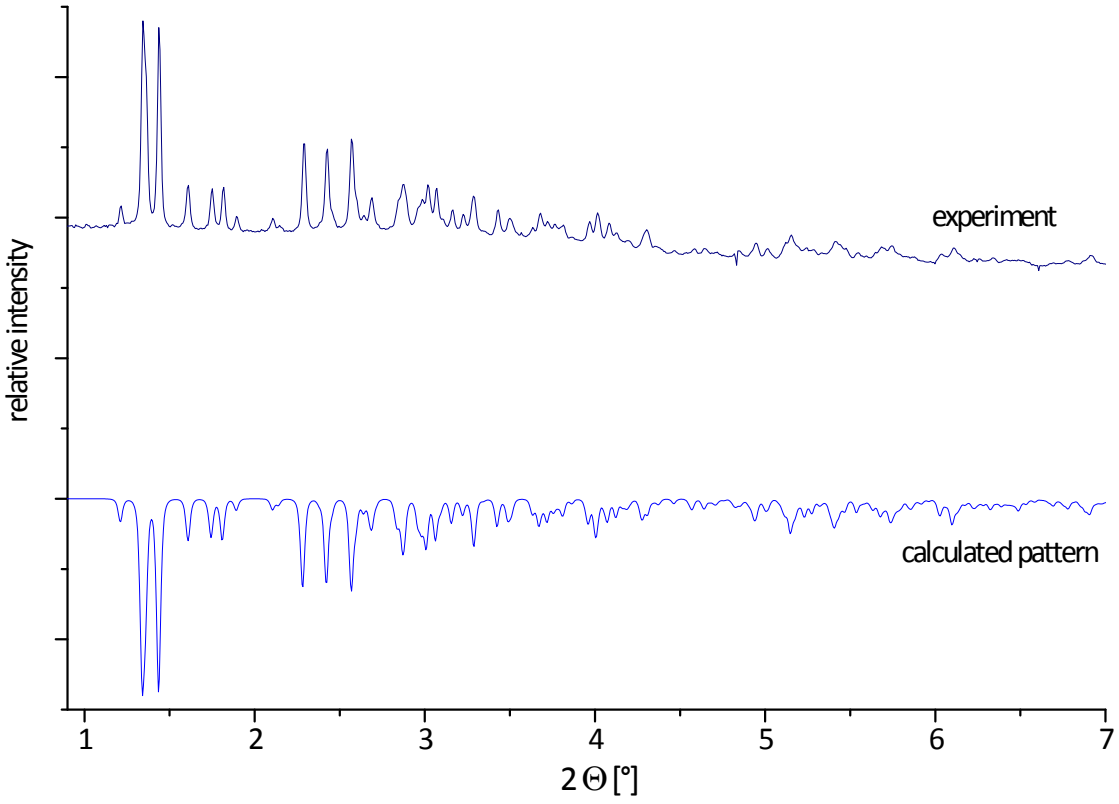

Figure S29: XRPD of $(BTMA)_2[Fe_4S_4Cl_2I_2]$; experiment with λ= 0.207203 Å synchrotron radiation (DESY, beam line P02.1, storage ring Petra III); calculated pattern based single crystal structure data.[1]

Literature

1. W. Saak and S. Pohl, *Z. Naturforsch.*, 1985, **40b**, 1105-1112.
2. A. O. Schüren, L. Carrella, E. Rothe, B. M. Ridgway, V. K. Gramm, F. Doctorovich, E. Rentschler, V. Schünemann, and A. Klein, *manuscript in preparation*, 2016.
3. A. Müller, N. H. Schladerbeck, E. Krickemeyer, H. Bögge, K. Schmitz, E. Bill, and A. X. Trautwein, *Z. Anorg. Allg. Chem.*, 1989, **570**, 7-36.